Spectral properties and the Kondo effect of cobalt adatoms on silicene

I. Weymann,[1,*] M. Zwierzycki,[2,†] and S. Krompiewski[2]
[1]*Faculty of Physics, Adam Mickiewicz University, 61-614 Poznań, Poland*
[2]*Institute of Molecular Physics, Polish Academy of Sciences, 60-179 Poznań, Poland*
(Received 26 May 2017; revised manuscript received 5 September 2017; published 29 September 2017)

In terms of the state-of-the-art first-principles computational methods combined with the numerical renormalization-group technique the spectroscopic properties of Co adatoms deposited on silicene are analyzed. By establishing an effective low-energy Hamiltonian based on first-principles calculations, we study the behavior of the local density of states of Co adatoms on external parameters, such as magnetic field and gating. It is shown that the Kondo resonance with a Kondo temperature of the order of a few kelvins can emerge by fine-tuning the chemical potential. The evolution and splitting of the Kondo peak with external magnetic field is also analyzed. Furthermore, it is shown that the spin polarization of an adatom's spectral function in the presence of magnetic field can be relatively large, and it is possible to tune the polarization and its sign by electrical means.

DOI: 10.1103/PhysRevB.96.115452

I. INTRODUCTION

The discovery of graphene, a two-dimensional (2D) honeycomb lattice of carbon atoms, in 2004 [1] spurred an interest in other 2D materials, especially those sharing graphene's crystal structure. The search was motivated by the hope that such materials would also share the defining feature of graphene, i.e., the presence of Dirac cones in their electronic structures [2]. The suppression of the backscattering characteristic of Dirac fermions should then lead to similarly high carrier mobilities [3–6] and possible use of graphene siblings in ultrafast electronic devices [7–11]. The continuously growing list of elements and compounds for which the existence of such graphene analogs was predicted theoretically and, in some cases, confirmed experimentally includes Si (so-called *silicene*) [12–18], Ge (*germanene*) [12,13], Sn (*stanene*) [19,20], Al (*aluminene*) [21,22], and hexagonal BN (*white graphene*) [23].

Of these, silicene is particularly interesting thanks to its compatibility with the current Si-based electronic technology. The first proof-of-concept field-effect transistor made out of silicene has already been demonstrated [24]. Many of the characteristic properties of graphene are predicted to be present also in its silicon counterpart. The band structure of free-standing silicene exhibits the expected Dirac cones [12], which can be preserved also on suitably selected substrates [25]. The zigzag edges of silicene nanoribbons are predicted to be spin polarized [12,26,27], just like in the case of graphene [2]. However, some notable differences also exist between the two materials. While graphene is planar, in silicene the two sublattices are shifted vertically (*buckling*) because of a larger in-plane lattice constant (weaker π bonds) and the element's preference for forming sp^3 hybrids (no graphite analog exists for Si). Consequently, the π and σ bands are hybridized. The spin-orbit (SO) interaction in silicene is three orders of magnitude stronger than in graphene and is responsible for a small 1.5 meV gap in the electronic structure [28,29]. This may lead to the realization of the spin Hall effect in experimentally accessible temperatures. The symmetry-breaking effect due to buckling opens an interesting possibility of fine-tuning the gap using the vertical electric field [30,31].

Another way of affecting the properties of 2D materials is by deposition of magnetic adatoms on the surface. In fact, the presence of impurities has been invoked to explain the spin-relaxation time in graphene [32]. Besides modification of material properties, individual magnetic adatoms themselves can pose very interesting objects to study. This is because strong coupling between localized states of adatoms and the band of a 2D material can result in various nontrivial effects. One such effect, which has been widely studied in the context of quantum dots and molecules, is undoubtedly the Kondo effect [33]. In this effect the magnetic moment of confined electrons, either in an adatom or a quantum dot, becomes screened by surrounding mobile electrons. This results in the formation of a resonance in the local density of states at the Fermi level [34]. The Kondo effect due to the presence of magnetic adatoms has already been considered in the case of graphene [35,36]. Moreover, the spectroscopic properties of Co adatoms on graphene have also been examined [37], and recently, the presence of the Kondo effect has been reported [38]. Thus, while there are several considerations of spectroscopic properties of magnetic adatoms on graphene, not much is known about the spectral features and, in particular, the Kondo effect for other 2D materials, such as silicene. The aim of this paper is therefore to shed light on the physics of Co adatoms on silicene, with an emphasis on the Kondo regime.

This paper is organized as follows. In Sec. II we discuss the first-principles methods used to determine the lowest-energy geometry and the density of states (DOS) of silicene with a Co adatom. Section III is devoted to numerical renormalization-group calculations. First, we formulate the effective Hamiltonian and describe the method, and then we discuss the numerical results. The paper is summarized in Sec. IV.

II. FIRST-PRINCIPLES CALCULATIONS

The first-principles calculations were performed using the generalized gradient approximation (GGA) of the density functional theory (DFT). The specific method applied was the full-potential linearized augmented plane wave (FLAPW) [39]

*weymann@amu.edu.pl
†maciej.zwierzycki@ifmpan.poznan.pl

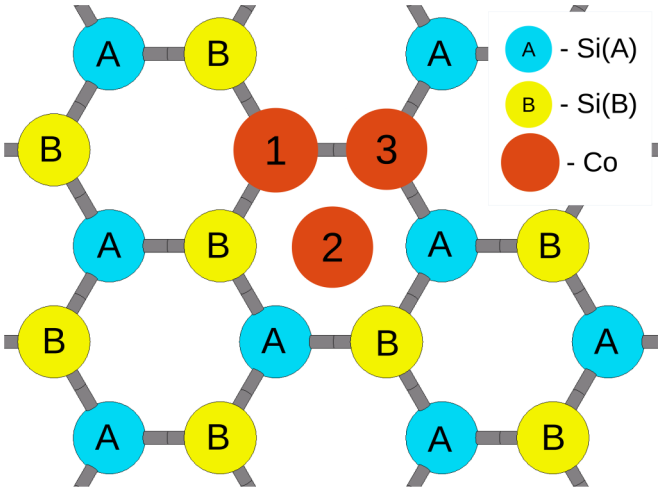

FIG. 1. Three possible high-symmetry positions of a Co adatom over the silicene plane. The two silicene sublattices are marked A and B, with B being the higher one. Note that because of the buckling positions 1 and 3 are nonequivalent.

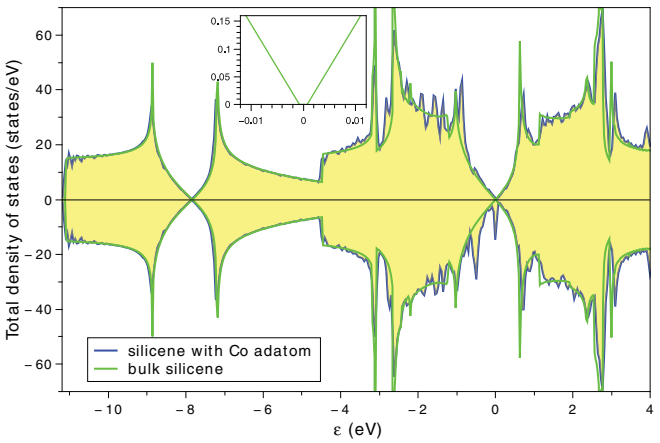

FIG. 2. The total density of states for a 7×7 supercell with a centrally located Co adatom on silicene. The green line corresponds to the density of states of pure silicene. The Fermi energy corresponds to $\varepsilon = 0$. The inset shows a small gap induced by the spin-orbit interaction in pure silicene.

as implemented in the WIEN2K package [40]. The Perdew-Burke-Ernzerhof parametrization [41] of the exchange potential was used in all the cases. The 2D Brillouin zone (2D BZ) integration was performed using the mesh densities corresponding to several hundreds k points (or more) in the single-unit 2D BZ. The convergence criteria for energy, charge per atom, and forces were set to 10^{-4} Ry, $10^{-3}e$, and 2 mRy/a.u., respectively. In all the calculations the silicene planes were separated by 14 Å, ensuring the lack of hopping between the neighboring planes.

In the first step the lattice constant and the sublattices' displacement of bulk silicene were optimized. For the lowest-energy configuration we found the in-plane lattice constant and the vertical displacement to be equal to $a = 3.86$ Å and $\Delta = 0.46$ Å [42], respectively, in good agreement with the previous calculations [12,28]. When the spin-orbit interactions were included in the calculations the small band gap of $\Delta E \approx 1.5$ meV separating the tips of the Dirac cones appeared in the band structure, also in good agreement with the literature [28].

Next, we compared three possible high-symmetry locations of the Co adatom over the silicene. These are indicated in Fig. 1 and include the locations over two nonequivalent lattice sites (1 and 3) and also the position over the center of the hexagon (2). The calculations were performed using 3×3 supercells with the full relaxation of the atomic positions within the supercell. It has been found, in agreement with earlier works [43,44], that the order of the total energies is as follows:

$$E_2 < E_1 < E_3;$$

that is, the central position 2 is the most favorable energetically, followed by the position over the "lower" sublattice A. The ground state is separated from the other two configurations by $\Delta E_{\mathrm{Tot}} \approx 0.17$ Ry. These conclusions were additionally confirmed by 4×4 calculations for cases 1 and 2 with the same overall results.

In order to make sure that the size of the supercell used is sufficiently large that the limit of the single impurity is reached we next studied the convergence of the magnetic moment and the local density of states (LDOS) of the Co adatom against the size of the supercell. Because of the huge computational costs involved, the structural relaxation was not performed during these calculations. Instead, we adopted the geometry obtained in 4×4 calculations for Co and its surroundings (up to $R = 8$ Å radius, corresponding to four coordination zones), embedding so-defined "cluster" into the bulk silicene. As the deviations of Si atoms from bulk positions were found to be negligible at this distance from Co, the procedure is reasonable. We found that both quantities stopped changing meaningfully when 7×7 (corresponding to the supercell lattice constant $a_{sc} = 27$ Å) or larger supercells were used. The total magnetic moment, located predominantly on Co, equals $1\mu_B$. We conclude therefore that the impurity can be effectively treated as a spin-1/2 in the Anderson model.

In the final step we calculated global and local DOS using a 7×7 supercell and including the spin-orbit coupling. The 2D BZ integration was performed at this point using a suitably dense mesh corresponding to 10^4 k points in the original 1×1 2D BZ. The results for the total DOS of the structure, together with the DOS of pure silicene, are presented in Fig. 2. In the vicinity of the adatom the hybridization effect comes into play, and it drastically rebuilds the LDOS. As a consequence, the DOS of the system with an adatom follows the same general outline as the DOS of pure silicene but with additional modulations visible in Fig. 2. The most notable of these is perhaps the sharp peak located exactly at the Fermi energy in the minority-spin channel. Analysis of the orbital contribution to the local density of states of cobalt shown in Fig. 3 indicates that the peak at the Fermi energy in the total DOS of the structure originates mainly from the $d_{3z^2-r^2}$ orbitals of the adatom.

III. NUMERICAL RENORMALIZATION-GROUP CALCULATIONS

A. Effective model

Based on the first-principles results we can now establish an effective Hamiltonian for the Co adatom on silicene. The

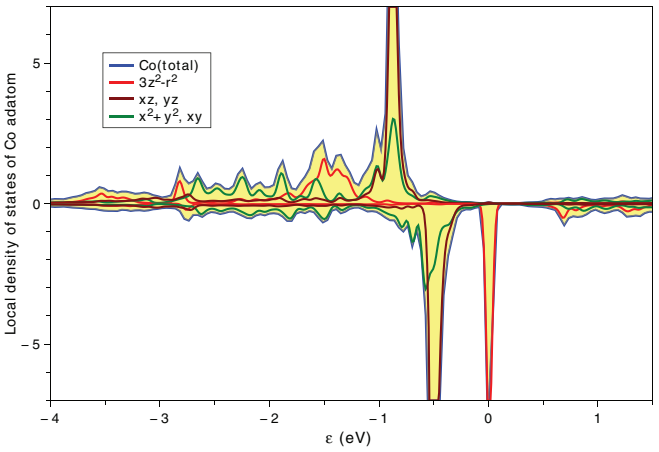

FIG. 3. The local density of states of a Co adatom. Both total and partial orbital-resolved contributions are indicated.

calculated magnetic moment of the adatom justifies the usage of a spin-1/2 single-impurity Anderson model [45]. In order to find the parameters of the effective single-orbital model we follow the procedure described in Ref. [46]. From the calculated occupancy of Co orbitals, $n_d \approx 7.8$ (in agreement with Ref. [44]), we conclude that charge fluctuations can occur between the states with 7, 8, and 9 electrons. Starting with the Anderson model with full fivefold degeneracy of the d-shell electrons, we note that in the mean-field approximation the energies of the respective charge states enumerated by j can be expressed as $E(j) = j\epsilon + Uj(j-1)/2$, where ϵ is an adatom on-site energy and U denotes the Coulomb correlations. Following Ref. [44], the latter parameter will be set equal to $U = 4$ eV. From the minimum-energy condition with respect to j we can estimate the on-site energy $\epsilon = (1/2 - n_d)U$. Focusing on consecutive energies of the states with 7, 8, and 9 electrons (with respect to the lowest energy), we can find from $\tilde{\varepsilon}_d = E(8) - E(7)$ and $2\tilde{\varepsilon}_d + \tilde{U} = E(9) - E(7)$ the parameters for the effective impurity Hamiltonian, $\tilde{\varepsilon}_d = -1.2$ eV, $\tilde{U} = U$, which has the following form:

$$H = H_{\text{band}} + H_{\text{imp}} + H_{\text{tun}}. \tag{1}$$

Here, $H_{\text{band}} = \sum_\sigma \int d\varepsilon\, \varepsilon\, c_\sigma^\dagger(\varepsilon) c_\sigma(\varepsilon)$ describes the electrons in silicene with the corresponding density of states (see Fig. 2). The second term models the adatom and is given by $H_{\text{imp}} = \sum_\sigma \tilde{\varepsilon}_d d_\sigma^\dagger d_\sigma + \tilde{U} d_\uparrow^\dagger d_\uparrow d_\downarrow^\dagger d_\downarrow + g\mu_B S_z B$, where $\tilde{\varepsilon}_d$ is the energy of an electron occupying the impurity and $\tilde{U}$ denotes the Coulomb correlation energy. The last term accounts for the Zeeman splitting, with B being the external magnetic field and S_z denoting the spin of the adatom. The operator $d_\sigma^\dagger$ creates a spin-σ electron on the adatom, and $c_\sigma^\dagger(\varepsilon)$ is the corresponding creation operator for spin-σ electrons in silicene. Finally, the coupling between the substrate and the adatom is modeled by the tunneling Hamiltonian $H_{\text{tun}} = \sum_\sigma \int d\varepsilon V \sqrt{\rho(\varepsilon)} [c_\sigma^\dagger(\varepsilon) d_\sigma + d_\sigma^\dagger c_\sigma(\varepsilon)]$, where V denotes the tunnel matrix elements assumed to be equal to $V = 0.65$ eV and $\rho(\varepsilon)$ is the density of states of bulk silicene (see Fig. 2). The parameter V has been evaluated by Harrison's scaling method [47] for the average Si-Co bond length $r = 2.45$ Å.

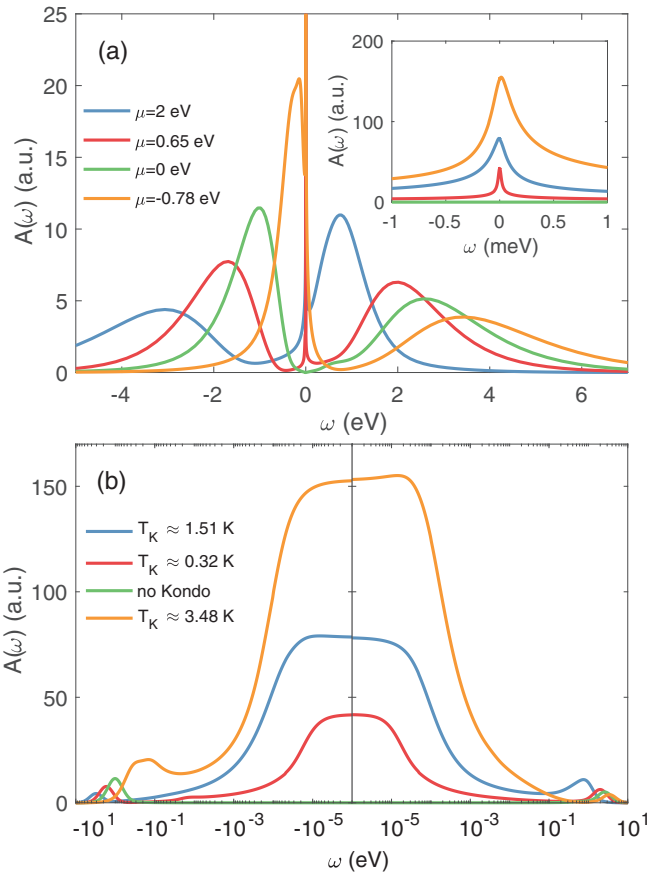

FIG. 4. The zero-temperature total spectral function of the Co adatom calculated by NRG for a few values of chemical potential μ, $E_F = \mu$, plotted on (a) linear and (b) logarithmic scales. The inset in (a) presents a close-up of the low-energy behavior where the Kondo effect can emerge. The associated Kondo temperatures, obtained from the half width at half maximum of the resonance in the spectral function, are indicated in the legend of (b). The parameters are $\tilde{U} = 4$ eV, $\tilde{\varepsilon}_d = -1.2$ eV, $V = 0.65$ eV, and $B = 0$. We also set $\hbar \equiv 1$.

Since we are interested in nonperturbative effects resulting from the hybridization of a Co adatom and silicene, to get the most accurate information about the system's spectral properties we employ the numerical renormalization group (NRG) method [48–50]. In NRG, the band is first discretized in a logarithmic way with a discretization parameter Λ. Then, such a discretized Hamiltonian is tridiagonalized numerically and transformed to a tight-binding Hamiltonian of the following form:

$$H_{\text{NRG}} = H_{\text{imp}} + \sum_\sigma V(d_\sigma^\dagger f_{0\sigma} + f_{0\sigma}^\dagger d_\sigma) + \sum_{n=0}^{\infty} \sum_\sigma [\epsilon_n f_{n\sigma}^\dagger f_{n\sigma} + t_n (f_{n\sigma}^\dagger f_{n+1\sigma} + f_{n+1\sigma}^\dagger f_{n\sigma})], \tag{2}$$

where $f_{n\sigma}^\dagger$ is the creation operator of an electron with spin σ on the nth site of the chain, t_n denotes the hopping integral, and ϵ_n is the on-site energy. In NRG calculations we assumed $\Lambda = 1.7$ and kept at least 1500 states at each iteration. To

obtain the most accurate results for the spectral functions, we also optimized the broadening parameter appropriately [51].

B. Discussion of numerical results

We now focus on the behavior of the spectral function of the Co adatom, $A_\sigma(\omega) = -\mathrm{Im}G^R_\sigma(\omega)/\pi$, where $G^R_\sigma(\omega)$ is the Fourier transform of the corresponding retarded Green's function, $G^R_\sigma(t) = -i\Theta(t)\langle\{d_\sigma(t), d^\dagger_\sigma(0)\}\rangle$. The total spectral function, $A(\omega) = A_\uparrow(\omega) + A_\downarrow(\omega)$, corresponds to the local density of states of the adatom, which can be experimentally examined with a weakly coupled probe, such as the tip of a scanning tunneling microscope.

1. *Spectral properties and the Kondo effect*

Because, experimentally, the position of the Fermi level can be adjusted by gating, in Fig. 4 we present the energy dependence of $A(\omega)$ calculated for different values of the chemical potential μ, $E_F = \mu$. Let us first focus on the case of no gating, $\mu = 0$. One can see that the total spectral function exhibits Hubbard resonances for $\omega = \tilde{\varepsilon}_d$ and $\omega = \tilde{\varepsilon}_d + \tilde{U}$. For typical spin-1/2 quantum impurity models, at low energies, the Kondo physics plays an important role [33]. In the Kondo effect the conduction electrons screen the impurity's spin, resulting in an additional resonance at the Fermi energy in the local density of states, the half width of which is related to the Kondo temperature T_K [34]. In the case considered here, however, due to the depletion of states at the Fermi energy the screening of the adatom spin is not possible, and consequently, the Kondo peak is not present (see Fig. 4 for $\mu = 0$).

One can consider if it is possible to reinstate the Kondo resonance by changing the chemical potential via gating. First of all, it can be seen that, quite naturally, by tuning μ the position of the Hubbard resonances changes accordingly (see Fig. 4). Moreover, by adjusting the Fermi energy, one can also considerably affect the low-energy behavior of the system. In fact, for values of μ selected in Fig. 4, a pronounced Kondo resonance develops. This can be clearly seen in Fig. 4(b), which shows the spectral function plotted on a logarithmic scale, as well as in the inset of Fig. 4(a), which presents a close-up of the low-energy behavior of $A(\omega)$. For the considered values of gating, there is a sufficient number of states at the Fermi energy to screen the adatom's spin. One can then observe the Kondo effect with a relatively large Kondo temperature, of the order of up to a few kelvins, as estimated from the half width at half maximum of the Kondo peak [see Fig. 4(b)].

To gain a deeper understanding of the effect of gating on the local density of states, we also analyze the behavior of the spectral function by continuously tuning the chemical potential. This is presented in Fig. 5, which shows the energy and chemical potential dependence of the local density of states, with the bottom panel zooming into the low-energy behavior of $A(\omega)$. First, we note that for $\mu \approx -1.2$ eV and $\mu \approx 2.8$ eV, the spectral function exhibits maxima related to resonant tunneling since then the empty and doubly occupied states of the adatom cross the Fermi energy (the adatom enters the mixed-valence regime). In the range of chemical potentials between these two values, the impurity effectively hosts a spin 1/2; Fig. 6(a) presents the chemical-potential dependence of the occupation $\langle n\rangle$ of the orbital level, where

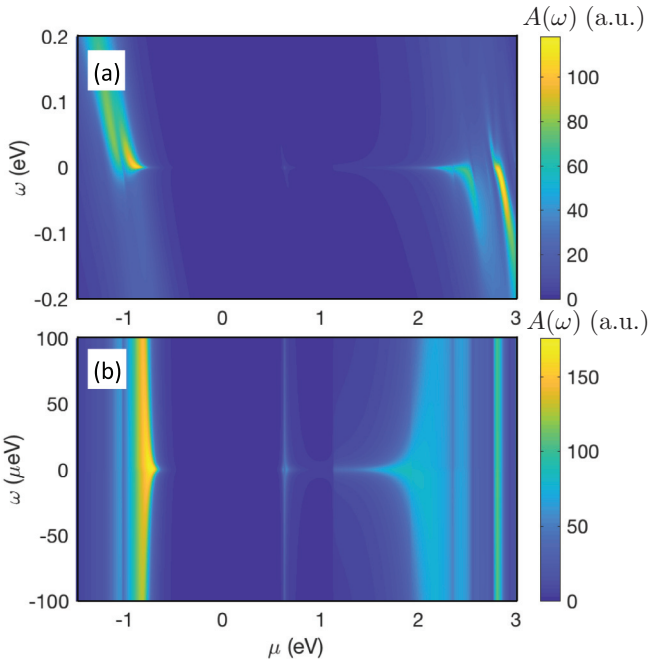

FIG. 5. (a) The total spectral function plotted versus energy ω and the chemical potential μ, $E_F = \mu$, calculated for the same parameters as in Fig. 4. (b) Close-up of the low-energy behavior of $A(\omega)$.

$n = \sum_\sigma d^\dagger_\sigma d_\sigma$. Consequently, one can expect that the Kondo effect will emerge if the number of states is sufficient to screen the impurity's spin. The occurrence of the Kondo resonance is thus strongly dependent on the hybridization, which changes with μ. As a matter of fact, one can indeed clearly identify regions where the resonance at the Fermi energy develops. These regions are more visible in Fig. 5(b), which shows the close-up of the low-energy behavior of the spectral function. From the inspection of this figure one can see that for values of chemical potential ranging from $\mu \approx 1.2$ eV to $\mu \approx 2.5$ eV, the Kondo resonance develops with Kondo temperature strongly dependent on μ. The Kondo temperature becomes enhanced for $\mu \approx 2$ eV, where $T_K \approx 1.5$ K. Moreover, a relatively large Kondo temperature can be also found for $\mu = -0.78$ eV, where $T_K \approx 3.48$ K [see Fig. 4(b)].

We recall that the Kondo temperature depends in an exponential fashion on the ratio of hybridization between the orbital level and the host and the Coulomb correlations [34]. Thus, from a theoretical point of view, if the host's density of states at the Fermi energy is finite, the Kondo peak should emerge even if DOS is very low. However, the corresponding Kondo temperature would then be extremely small, and thus, the Kondo peak would be completely undetectable experimentally. In Fig. 6(b) we present the chemical-potential dependence of the spectral function at $\omega = 0$ for several experimentally relevant values of temperature. By looking at the orbital-level occupation [Fig. 6(a)], one can recognize an enhanced spectral function due to resonant tunneling in the mixed-valence regime and due to the Kondo effect in the local-moment regime. Moreover, one can also inspect how quickly the Kondo correlations become smeared out by thermal fluctuations, which is especially visible in the range of μ from $\mu \approx 1.2$ eV to $\mu \approx 2.5$ eV.

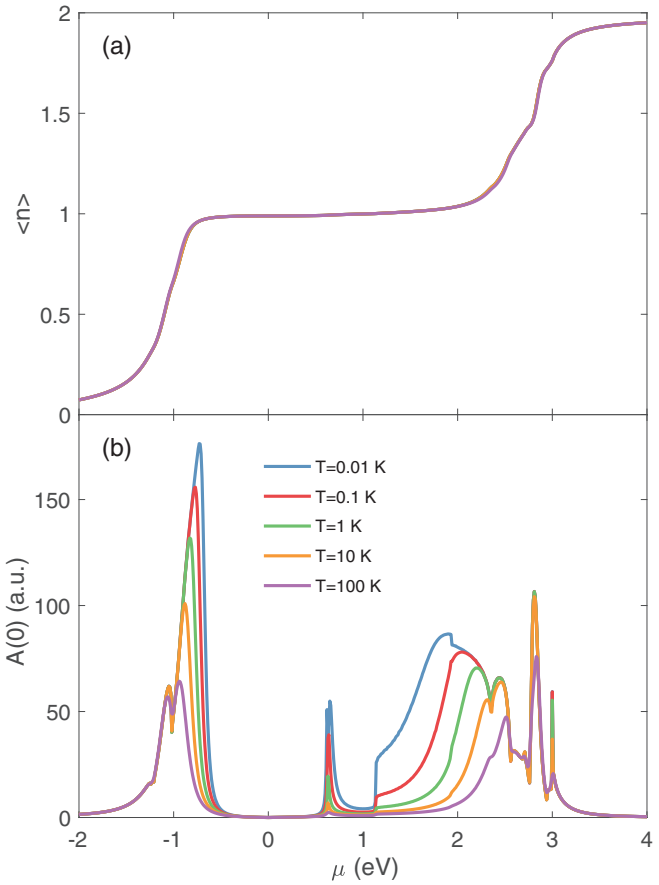

FIG. 6. (a) The occupation of the orbital level $\langle n \rangle$ and (b) the spectral function at $\omega = 0$ $A(0)$ plotted as a function of chemical potential μ and calculated for different temperatures, as indicated. The other parameters are the same as in Fig. 4. Note that the occupation hardly depends on temperature since the energy scales of the adatom are still much larger than the considered temperatures.

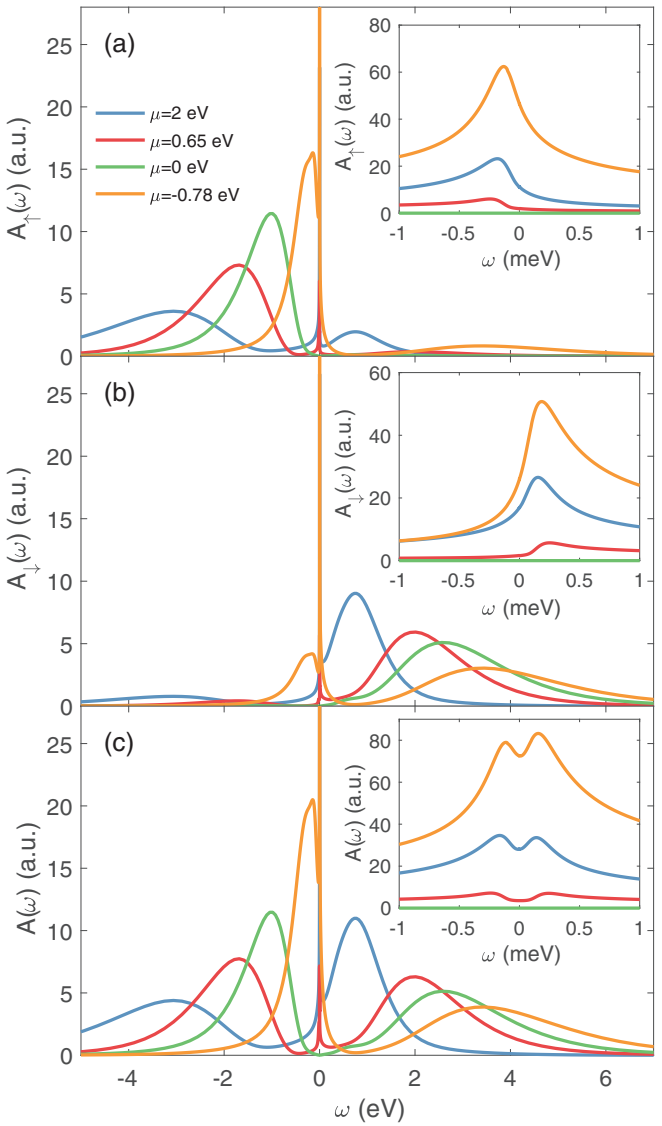

FIG. 7. The zero-temperature (a) spin-up, (b) spin-down, and (c) total spectral functions for different values of the chemical potential, as indicated, calculated in the presence of external magnetic field $B = 2$ T. The insets present close-ups of the low-energy behavior of the spectral function. Parameters are the same as in Fig. 4, and we assumed the g factor $g = 2$.

2. *Effect of external magnetic field*

Let us now consider how external magnetic field affects the behavior of the local density of states of a Co adatom. The energy dependence of the spin-resolved and total spectral function calculated in the presence of external magnetic field $B = 2$ T is depicted in Fig. 7, where the insets show a close-up of the low-energy behavior of $A(\omega)$. First of all, one can see that magnetic field strongly affects the behavior of the spectral function. An important observation is a strong spin polarization of Hubbard resonances: $A_\uparrow$ ($A_\downarrow$) becomes suppressed for $\omega > 0$ ($\omega < 0$). Moreover, magnetic field also has a strong effect on the low-energy behavior of $A(\omega)$: the Kondo resonance becomes split if the Zeeman energy E_Z becomes larger than $k_B T_K$, $E_Z = g\mu_B B \gtrsim k_B T_K$. The spin polarization of the spectral function can be clearly seen in Figs. 7(a) and 7(b), while the splitting of the Kondo peak is nicely visible in the inset of Fig. 7(c). We note that the largest suppression of the Kondo peak occurs for $\mu = 0.65$ eV. For this value of gating we estimated $T_K \approx 0.32$ K, which is smaller than for the case of $\mu = 2$ eV and $\mu = -0.78$ eV. Consequently, larger suppression of the Kondo resonance is observed for smaller T_K since the condition $E_Z \gtrsim k_B T_K$ is then better satisfied. We also notice that the effect of splitting and suppression of the Kondo peak in the presence of magnetic field is in fact similar to the effect of an exchange-field splitting of the orbital level caused by the presence of ferromagnetic correlations [52–56]. Thus, if, due to the proximity effect of the magnetic substrate, the density of states of silicene becomes spin polarized, the Kondo effect may also be split and suppressed even in the absence of magnetic field.

It is also interesting to analyze the energy and chemical-potential dependence of the local density of states for several values of external magnetic field. This is presented in Fig. 8, which shows $A(\omega)$ for $B = 1,2,5$ T. In Fig. 8 we focus on the low-energy regime, where the Kondo effect can emerge, and the interplay between the Zeeman splitting and Kondo correlations is clearly revealed. One can see that, depending

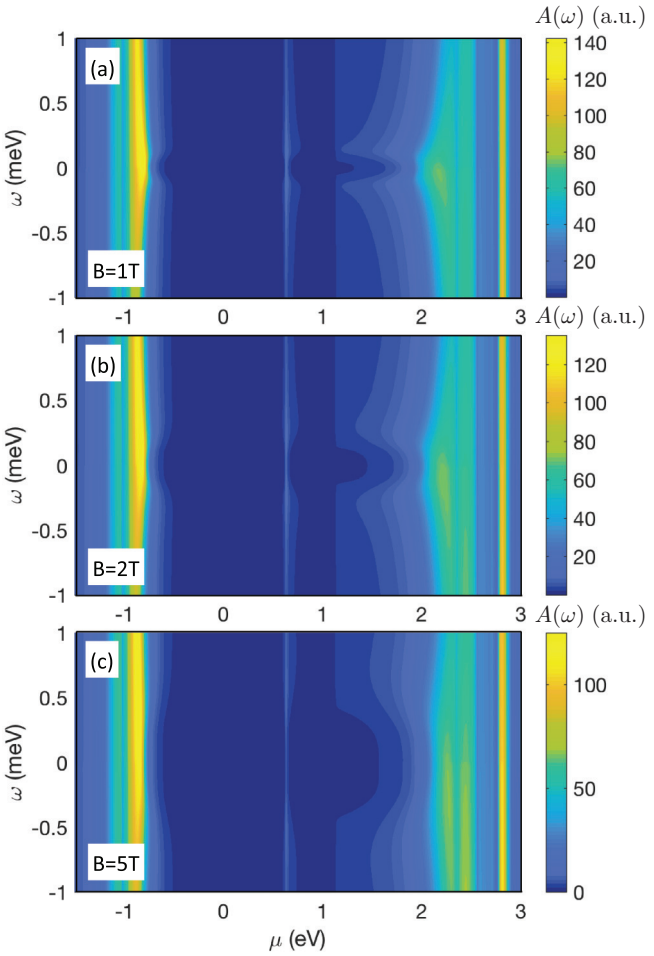

FIG. 8. The energy and chemical-potential dependence of the total spectral function for different values of external magnetic field: (a) $B = 1$ T, (b) $B = 2$ T, and (c) $B = 5$ T. The other parameters are the same as in Fig. 4.

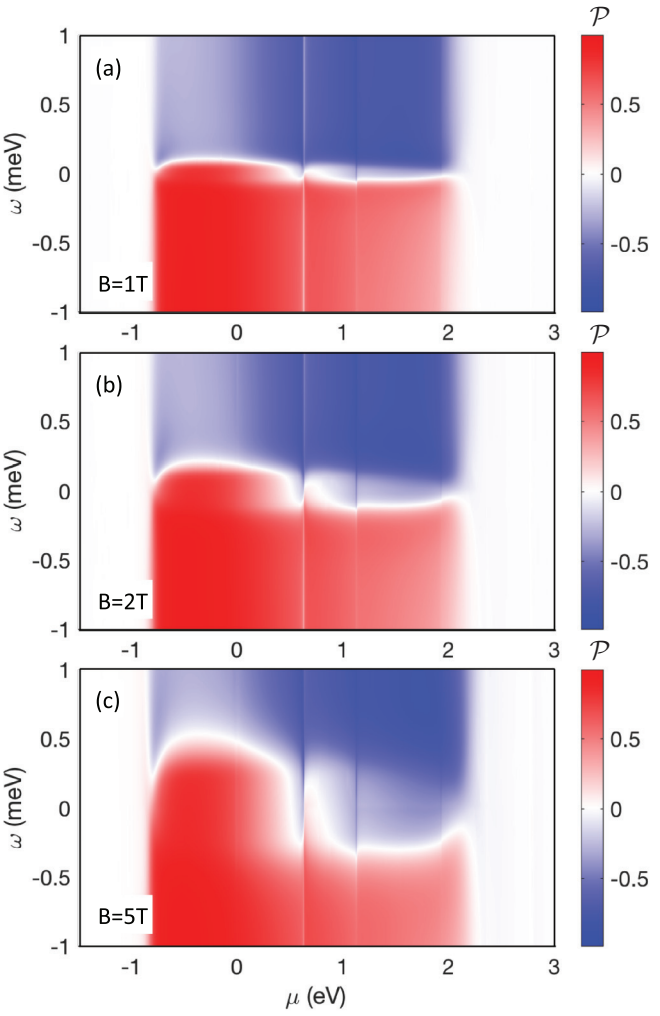

FIG. 9. The energy and chemical-potential dependence of the spin polarization of the spectral function, $\mathcal{P} = [A_\uparrow(\omega) - A_\downarrow(\omega)]/A(\omega)$, calculated for different values of external magnetic field: (a) $B = 1$ T, (b) $B = 2$ T, and (c) $B = 5$ T. The other parameters are the same as in Fig. 4.

on the value of external magnetic field and gating, the Kondo resonance can become split and suppressed. This is especially visible for $\mu = 1.5$ eV, where, with increasing B, one shifts the position of the split Kondo peaks. Moreover, there are values of μ, especially those close to the mixed-valence regime, where the magnetic field is not strong enough to suppress the Kondo resonance (see Fig. 8).

The effect of external magnetic field can be better revealed when one considers the spin polarization of the spectral function, which is defined as $\mathcal{P} = [A_\uparrow(\omega) - A_\downarrow(\omega)]/A(\omega)$. The dependence of the spin polarization on energy ω and chemical potential μ for a few values of magnetic field is shown in Fig. 9. This figure is generated for the same values of B as those considered in Fig. 8, again focusing on the low-energy behavior. When the impurity is either empty or doubly occupied, the spin polarization is suppressed and approaches zero. Its behavior, however, becomes completely changed in the local-moment regime (see Fig. 9). The first observation is that $\mathcal{P}$ can change sign around $\omega = 0$, and such a sign flip occurs in the regime where the impurity is occupied by a single electron. This effect is associated with the spin splitting of the adatom orbital due to the Zeeman field. One can notice that for higher energies the spectral function becomes fully spin polarized, $\mathcal{P} \approx 1$ for $\omega < 0$ and $\mathcal{P} \approx -1$ for $\omega > 0$. Interestingly, it can also be seen that the interplay of finite Zeeman splitting and the density of states of silicene can result in a sign change of the spin polarization at $\omega = 0$ around $\mu = 0.5$ eV, which is clearly visible for $B = 5$ T [see Fig. 9(c)]. At low energies and for $\mu \lesssim 0.5$ eV ($\mu \gtrsim 0.5$ eV), $\mathcal{P}$ becomes positive (negative).

Finally, in Fig. 10 we study the evolution of the splitting of the Kondo peak with external magnetic field. Figure 10 is calculated for selected values of the chemical potential, the same ones as considered in Fig. 7. It can be seen that the Kondo peak becomes suppressed when magnetic field is so strong that the condition $E_Z \gtrsim k_B T_K$ is fulfilled. Thus, the suppression occurs first for the case of $\mu = 0.65$ eV, while larger field is needed to destroy the Kondo resonance for

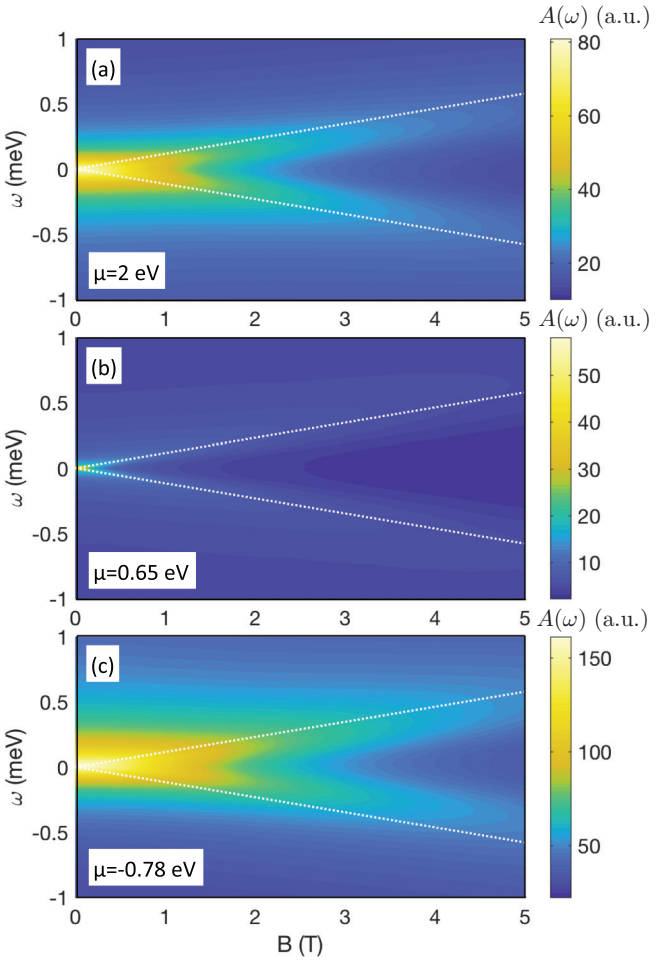

FIG. 10. The spectral function plotted as a function of energy and magnetic field for selected values of chemical potential for which a pronounced Kondo peak develops in the absence of magnetic field: (a) $\mu = 2$ eV, (b) $\mu = 0.65$ eV, and (c) $\mu = -0.78$ eV. The dotted lines mark the Zeeman energy $E_Z = \pm g\mu_B B$. The other parameters are the same as in Fig. 4.

the other two cases (see Fig. 10). When magnetic field is large enough that $E_Z \gtrsim k_B T_K$, $A(0)$ becomes suppressed, and the spectral function shows only side peaks, which occur exactly at the spin-flip excitation energy $\omega = \pm E_Z$. The position of those side peaks depends thus linearly on magnetic field, which can be nicely seen in Fig. 10, where the dotted lines mark the Zeeman energy E_Z.

IV. CONCLUSIONS

We have theoretically considered the spectroscopic properties and the Kondo effect of Co adatoms on silicene. By using the first-principles calculations, we have determined the total density of states of the Co-silicene system and estimated the orbital-level occupancy together with the magnetic moment of Co. Our DFT results allowed us to formulate an effective low-energy Hamiltonian for spin-1/2 impurity, which was further used to analyze the spectral properties of Co adatoms. This analysis was performed by employing the numerical renormalization-group method with a nonconstant density of states. We focused on the behavior of the local density of states (spectral function), which can be probed experimentally by using scanning tunneling spectroscopy. The analysis involved the effects of external magnetic field and gating of silicene. We showed that by appropriately tuning the parameters one can obtain clear signatures of the Kondo effect. We also analyzed the evolution and splitting of the Kondo resonance with an external magnetic field. Finally, we studied the spin polarization of the spectral function in the presence of magnetic field, whose magnitude and sign were found to greatly depend on the position of the chemical potential.

ACKNOWLEDGMENTS

I.W. acknowledges discussions with C. P. Moca. This work is supported by the Polish National Science Centre with funds awarded through Decision No. DEC-2013/10/M/ST3/00488.

[1] K. S. Novoselov, A. K. Geim, S. V. Morozov, D. Jiang, Y. Zhang, S. V. Dubonos, I. V. Grigorieva, and A. A. Firsov, Science **306**, 666 (2004).
[2] A. H. Castro Neto, F. Guinea, N. M. R. Peres, K. S. Novoselov, and A. K. Geim, Rev. Mod. Phys. **81**, 109 (2009).
[3] K. S. Novoselov, A. K. Geim, S. V. Morozov, D. Jiang, M. I. Katsnelson, I. V. Grigorieva, S. V. Dubonos, and A. A. Firsov, Nature (London) **438**, 197 (2005).
[4] Y. B. Zhang, Y. W. Tan, H. L. Stormer, and P. Kim, Nature (London) **438**, 201 (2005).
[5] K. I. Bolotin, K. J. Sikes, J. Hone, H. L. Stormer, and P. Kim, Phys. Rev. Lett. **101**, 096802 (2008).
[6] X. Du, I. Skachko, A. Barker, and E. Y. Andrei, Nat. Nanotechnol. **3**, 491 (2008).
[7] Y.-M. Lin, K. A. Jenkins, A. Valdes-Garcia, J. P. Small, D. B. Farmer, and P. Avouris, Nano Lett. **9**, 422 (2009).
[8] L. Liao, Y.-C. Lin, M. Bao, R. Cheng, J. Bai, Y. Liu, Y. Qu, K. L. Wang, Y. Huang, and X. Duan, Nature (London) **467**, 305 (2010).
[9] Y.-M. Lin, A. Valdes-Garcia, S.-J. Han, D. B. Farmer, I. Meric, Y. Sun, Y. Wu, C. Dimitrakopoulos, A. Grill, P. Avouris, and K. A. Jenkins, Science **332**, 1294 (2011).
[10] F. Schwierz, Nat. Nanotechnol. **5**, 487 (2010).
[11] W. Kim, P. Pasanen, J. Riikonen, and H. Lipsanen, Nanotechnology **23**, 115201 (2012).
[12] S. Cahangirov, M. Topsakal, E. Aktürk, H. Şahin, and S. Ciraci, Phys. Rev. Lett. **102**, 236804 (2009).
[13] S. Lebègue and O. Eriksson, Phys. Rev. B **79**, 115409 (2009).
[14] P. Vogt, P. De Padova, C. Quaresima, J. Avila, E. Frantzeskakis, M. C. Asensio, A. Resta, B. Ealet, and G. L. Lay, Phys. Rev. Lett. **108**, 155501 (2012).
[15] B. Feng, Z. Ding, S. Meng, Y. Yao, X. He, P. Cheng, L. Chen, and K. Wu, Nano Lett. **12**, 3507 (2012).
[16] C.-L. Lin, R. Arafune, K. Kawahara, N. Tsukahara, E. Minamitani, Y. Kim, N. Takagi, and M. Kawai, Appl. Phys. Express **5**, 045802 (2012).

[17] H. Jamgotchian, Y. Colignon, N. Hamzaoui, B. Ealet, J. Y. Hoarau, B. Aufray, and J. P. Bibérian, J. Phys. Condens. Matter **24**, 172001 (2012).
[18] D. Chiappe, C. Grazianetti, G. Tallarida, M. Fanciulli, and A. Molle, Adv. Mater. **24**, 5088 (2012).
[19] J. C. Garcia, D. B. de Lima, L. V. C. Assali, and J. F. Justo, J. Phys. Chem. C **115**, 13242 (2011).
[20] S. Saxena, R. P. Chaudhary, and S. Shukla, Sci. Rep. **6**, 31073 (2016).
[21] C. Kamal, A. Chakrabarti, and M. Ezawa, New J. Phys. **17**, 083014 (2015).
[22] J. Yuan, N. Yu, K. Xue, and X. Miao, Appl. Surf. Sci. **409**, 85 (2017).
[23] A. Nag, K. Raidongia, K. P. S. S. Hembram, R. Datta, U. V. Waghmare, and C. N. R. Rao, ACS Nano **4**, 1539 (2010).
[24] L. Tao, E. Cinquanta, D. Chiappe, C. Grazianetti, M. Fanciulli, M. Dubey, A. Molle, and D. Akinwande, Nat. Nanotechnol. **10**, 227 (2015).
[25] R. Quhe, Y. Yuan, J. Zheng, Y. Wang, Z. Ni, J. Shi, D. Yu, J. Yang, and J. Lu, Sci. Rep. **4**, 5476 (2014).
[26] I. Weymann, J. Barnaś, and S. Krompiewski, Phys. Rev. B **92**, 045427 (2015).
[27] I. Weymann and S. Krompiewski, Phys. Rev. B **94**, 235441 (2016).
[28] C.-C. Liu, W. Feng, and Y. Yao, Phys. Rev. Lett. **107**, 076802 (2011).
[29] C.-C. Liu, H. Jiang, and Y. Yao, Phys. Rev. B **84**, 195430 (2011).
[30] N. D. Drummond, V. Zólyomi, and V. I. Fal'ko, Phys. Rev. B **85**, 075423 (2012).
[31] Z. Ni, Q. Liu, K. Tang, J. Zheng, J. Zhou, R. Qin, Z. Gao, D. Yu, and J. Lu, Nano Lett. **12**, 113 (2012).
[32] D. Kochan, M. Gmitra, and J. Fabian, Phys. Rev. Lett. **112**, 116602 (2014).
[33] J. Kondo, Prog. Theor. Phys. **32**, 37 (1964).
[34] A. C. Hewson, *The Kondo Problem to Heavy Fermions* (Cambridge University Press, Cambridge, 1997).
[35] T. O. Wehling, A. V. Balatsky, M. I. Katsnelson, A. I. Lichtenstein, and A. Rosch, Phys. Rev. B **81**, 115427 (2010).
[36] L. Fritz and M. Vojta, Rep. Prog. Phys. **76**, 032501 (2013).
[37] V. W. Brar, R. Decker, H.-M. Solowan, Y. Wang, L. Maserati, K. T. Chan, H. Lee, Ç. O. Girit, A. Zettl, S. G. Louie, M. L. Cohen, and M. F. Crommie, Nat. Phys. **7**, 43 (2011).
[38] J. Ren, H. Guo, J. Pan, Y. Y. Zhang, X. Wu, H.-G. Luo, S. Du, S. T. Pantelides, and H.-J. Gao, Nano Lett. **14**, 4011 (2014).
[39] D. Singh, *Planewaves, Pseudopotentials, and the LAPW Method* (Springer, New York, 2006).
[40] P. Blaha, K. Schwarz, G. Madsen, D. Kvasnicka, and J. Luitz, in *WIEN2k, an Augmented Plane Wave + Local Orbitals Program for Calculating Crystal Properties*, edited by K. Schwarz (Technische Universität Wien, Vienna, 2001).
[41] J. P. Perdew, K. Burke, and M. Ernzerhof, Phys. Rev. Lett. **77**, 3865 (1996).
[42] This corresponds to the interatomic distance of $d_{Si-Si} = 2.28$ Å.
[43] X. Lin and J. Ni, Phys. Rev. B **86**, 075440 (2012).
[44] T. P. Kaloni, N. Singh, and U. Schwingenschlögl, Phys. Rev. B **89**, 035409 (2014).
[45] P. W. Anderson, Phys. Rev. **124**, 41 (1961).
[46] O. Újsághy, J. Kroha, L. Szunyogh, and A. Zawadowski, Phys. Rev. Lett. **85**, 2557 (2000).
[47] W. A. Harrison, *Electronic Structure and the Properties of Solids* (Dover, New York, 1980).
[48] K. G. Wilson, Rev. Mod. Phys. **47**, 773 (1975).
[49] O. Legeza, C. P. Moca, A. I. Tóth, I. Weymann, and G. Zarand, arXiv:0809.3143; the open access Budapest Flexible DM-NRG code is available at http://www.phy.bme.hu/~dmnrg/
[50] R. Bulla, T. A. Costi, and T. Pruschke, Rev. Mod. Phys. **80**, 395 (2008).
[51] R. Žitko and T. Pruschke, Phys. Rev. B **79**, 085106 (2009).
[52] J. Martinek, Y. Utsumi, H. Imamura, J. Barnaś, S. Maekawa, J. König, and G. Schön, Phys. Rev. Lett. **91**, 127203 (2003).
[53] J. R. Hauptmann, J. Paaske, and P. E. Lindelof, Nat. Phys. **4**, 373 (2008).
[54] M. Gaass, A. K. Hüttel, K. Kang, I. Weymann, J. von Delft, and C. Strunk, Phys. Rev. Lett. **107**, 176808 (2011).
[55] I. Weymann, Phys. Rev. B **83**, 113306 (2011).
[56] S. Csonka, I. Weymann, and G. Zarand, Nanoscale **4**, 3635 (2012).